

Gamma-Ray Bursts in Pulsar Wind Bubbles: Putting the Pieces Together

Jonathan Granot¹ and Dafne Guetta²

ABSTRACT

We present the main observational features expected for Gamma-Ray Bursts (GRBs) that occur inside pulsar wind bubbles (PWBs). This is the most natural outcome of supranova model, where initially a supernova explosion takes place, leaving behind a supra-massive neutron star, which loses its rotational energy over a time t_{sd} and collapses to a black hole, triggering a GRB explosion. We find that the time delay t_{sd} between the supernova and GRB events is the most important parameter that determines the behavior of the system. We consider the afterglow and prompt GRB emission, as well as the direct emission from the PWB. The observational signatures for different ranges in t_{sd} are described and joined together into one coherent framework. Constraints on the model are derived for a spherical PWB, from the lack of direct detection of emission from the PWB together with current afterglow observations. For very low values of $t_{\text{sd}} \lesssim 1$ hr the supranova model reduces to the collapsar model. Values of $0.4 \text{ yr} \lesssim t_{\text{sd}} \lesssim 1 \text{ yr}$ are required to produce the iron lines seen in several X-ray afterglows. However, we find that for a simple spherical model, this implies no detectable radio afterglow, a small jet break time and non-relativistic transition time, in disagreement with observations for some of the GRBs with X-ray lines. These discrepancies with the observations may be reconciled by resorting to a non-spherical geometry. We find that light element lines, that have been recently detected in a few X-ray afterglows, are expected to dominate over iron lines for small t_{sd} , while for large t_{sd} the situation is reversed. Finally, we predict that the inverse Compton upscattering of the PWB photons by the relativistic electrons of the afterglow (external Compton) should lead to high energy emission during the early afterglow that might explain the GeV photons detected by EGRET for a few GRBs, and should be detectable by future missions such as GLAST.

Subject headings: gamma rays: bursts—pulsars: general—supernova remnants—radiation mechanisms: nonthermal

¹Institute for Advanced Study, Olden Lane, Princeton, NJ 08540; granot@ias.edu

²Osservatorio astrofisico di Arcetri, L.E. Fermi 2, Firenze, Italy; dafne@arcetri.astro.it

1. Introduction

Despite the large progress in Gamma-Ray Burst (GRB) research over the last several years, the identity of their progenitors is still one of the most interesting open questions. Progenitor models of GRBs are divided into two main categories. The first category involves the merger of a binary system of compact objects, such as a double neutron star (NS-NS, Eichler et al. 1989), a neutron star and a black hole (NS-BH, Narayan, Pacyński & Piran 1992) or a black hole and a Helium star or a white dwarf (BH-He, BH-WD, Fryer & Woosley 1998; Fryer, Woosley & Hartmann 1999). The second category involves the death of a massive star. It includes the failed supernova (Woosley 1993) or hypernova (Pacyński 1998) models, where a black hole is created promptly, and a large accretion rate from a surrounding accretion disk (or torus) feeds a strong relativistic jet in the polar regions. This type of model is known as the collapsar model. An alternative model within this second category is the supranova model (Vietri & Stella 1998), where a massive star explodes in a supernova and leaves behind a supra-massive neutron star (SMNS) which after a time delay of t_{sd} , loses its rotational energy and collapses to a black hole, triggering the GRB event. Long GRBs (with a duration $\gtrsim 2$ s) are usually attributed to the second category of progenitors, while short GRBs are attributed to the first category. In all the different scenarios mentioned above, the final stage of the process consists of a newly formed black hole with a large accretion rate from a surrounding torus, and involve a similar energy budget ($\lesssim 10^{54}$ ergs).

In this work we concentrate on the supranova progenitor model, focusing on its possible observational signatures. The original motivation for this model was to provide a relatively baryon clean environment for the GRB jet. As it turned out, it also seemed to naturally accommodate the later detection of iron lines in several X-ray afterglows (Lazzati, Campana, & Ghisellini 1999; Piro et al. 2000; Vietri et al. 2001). It has recently been suggested that the most natural mechanism by which the SMNS can lose its rotational energy is through a strong pulsar type wind, between the supernova and the GRB events, which typically creates a pulsar wind bubble (PWB), also referred to as a plerion (Königl & Granot 2002, KG hereafter; Inoue, Guetta & Pacini 2002).

In an accompanying paper (Guetta & Granot 2002, GG hereafter) we study in detail the observational implications of GRBs occurring inside a PWB. We find that the most important parameter that determines the behavior of the system is the time delay, t_{sd} , between the supernova and GRB events. The value of t_{sd} is given by the typical timescale on which the SMNS loses its rotational energy due to magnetic dipole radiation (see Eq. 2 of GG) and depends mainly on the polar surface magnetic field strength of the SMNS, B_* (since its mass, radius and spin period are constrained to a much smaller range of possible values). For $B_* \sim 10^{12} - 10^{13}$ G, t_{sd} ranges between a few weeks and several years. However,

a larger range in B_* , and correspondingly in t_{sd} , seems plausible. We therefore consider t_{sd} as a free parameter. Another important parameter is the Lorentz factor, γ_w , of the pulsar wind, emanating from the SMNS, which is expected to be in the range $\sim 10^4 - 10^7$ (KG).

An important difference between our analysis and previous works (KG; Inoue, Guetta & Pacini 2002) is that we allow for a proton component in the pulsar wind, that carries a significant fraction of its energy. In contrast to the e^\pm component, the internal energy of the protons in the shocked wind is not radiated away, and therefore a large fraction of the energy in the pulsar wind ($\sim 10^{53}$ ergs) is always left in the PWB. This implies that even for a fast cooling PWB, the radius of the wind termination shock is significantly smaller than the radius of the supernova remnant (SNR) shell, and that the afterglow shock typically becomes non-relativistic before it reaches the outer boundary of the PWB. In the standard model the external medium is composed of cold protons and electrons (in equal numbers), and has a density profile that scales with the distance from the source as r^{-k} , where $k = 0$ for an ISM and $k = 2$ for a stellar wind. In our scenario, the external medium is made up of hot protons and cold e^\pm pairs, where there are $\sim 10^3$ times more pairs than protons. Nevertheless, the protons hold most of the energy in the PWB due to their large internal energy, which also dominates the effective density that is responsible for the deceleration of the afterglow shock. The value of k for our model ranges between $k = 0$, that is similar to an ISM, and $k = 1$, that is intermediate between an ISM and a stellar wind.

In this *Letter* we relate between the different aspects of this model, and focus on the observational implications that arise from different values of t_{sd} . We describe the main results and put them into one coherent picture, while for the detailed calculations we refer the reader to GG. We show that a simple spherical model cannot account for the X-ray features detected in several afterglows, together with the typical afterglow emission that was observed in the same afterglows. On the other hand, if the X-ray features turn out not to be real, then a simple spherical model is compatible with all current observations, and still holds many advantages compared to other progenitor models. It has been pointed out in previous works that an asymmetry of the remnant is required in order to explain the iron lines (Lazzati, Campana, & Ghisellini 1999; Vietri et al. 2001; KG) and its necessity is strengthened by the detailed analysis presented in GG, whose main points are reported here. We show that an elongated PWB can in principle account for the X-ray line together with the usual afterglow emission. In this paper we also show that this model with a modified geometry can in principle account for the iron lines, as well as the recent detection of X-ray lines from light elements (Reeves et al. 2001; Watson et al. 2002). We find that a small t_{sd} favors light element lines, while a large t_{sd} favors iron lines.

In §2 we consider the effects of different t_{sd} on the possibility for direct detection of the

plerion emission, the prompt GRB and the afterglow emission, and address the conditions that are required for the production of iron lines and not detecting the plerion emission. In §3 we discuss the conditions required for the production of light element lines, that have been recently observed in a few afterglows, compared to iron lines. The high energy emission due to the upscattering of the plerion photons by the relativistic electrons in the afterglow shock (external Compton, EC hereafter) is discussed in §4. In §5 we outline how some of the constraints on the model may be eased if the PWB is elongated, instead of spherical. Our conclusions are given in §6.

2. The Behavior of a Spherical PWB for Different Time Delays

In this section we go over the main observational signatures of the PWB model, following the different regimes in t_{sd} :

1. For extremely small values of $t_{\text{sd}} < t_{\text{col}} = R_{\star}/\beta_b c \approx 0.9 R_{\star,13} \beta_{b,-1}^{-1}$ hr, where $R_{\star} = 10^{13} R_{\star,13}$ cm is the radius of the progenitor star (before it explodes in a supernova), the stellar envelope does not have enough time to increase its radius considerably before the GRB goes off, and the supranova model reduces to the collapsar model. In this respect, the collapsar model may be seen as a special case of the supranova model. Such low values of t_{sd} might be achieved if the SMNS is not rotating uniformly, as differential rotation may amplify the magnetic field to very large values, or if the dominant energy loss mechanism is gravitational radiation, which can cause significant energy loss on a short time scale.
2. When $t_{\text{col}} < t_{\text{sd}} < t_{\text{IS}} \sim 16$ days (e.g. GG) the deceleration radius is smaller than the radius for internal shocks. In this case the kinetic energy of the GRB ejecta is dissipated through an external shock that is driven into the shocked pulsar wind, before internal shocks that result from variability within the outflow have time to occur.
3. If $t_{\text{IS}} < t_{\text{sd}} < t_{\tau} \sim 0.4$ yr, internal shocks can occur inside the PWB, but the SNR shell is still optically thick to Thomson scattering, and the radiation from the plerion, the prompt GRB and the afterglow cannot escape and reach the observer. If the SNR shell is clumpy (possibly due to the Rayleigh-Taylor instability, see §2 of GG), then the Thomson optical depth in the under-dense regions within the SNR shell may decrease below unity at t_{sd} somewhat smaller than t_{τ} , enabling some of the radiation from the plerion to escape. The only signatures that we expect for this range of t_{sd} are the neutrino emission due to p-p collisions or photo-meson interactions, and high energy photons above $0.5 (t_{\text{sd}}/t_{\tau})^{-2}$ MeV, whose cross section for scattering on the SNR electrons is reduced due to the Klein-Nishina effect. Predictions for the neutrino and high energy photon fluxes from this kind of environ-

ment as well as the mechanisms responsible for this emission will be discussed in detail in a forthcoming paper (Granot & Guetta 2002, in preparation)

4. For $t_\tau < t_{\text{sd}} < t_{\text{Fe}} \sim 1$ yr the SNR shell has a Thomson optical depth smaller than unity, but the optical depth for the iron line features is still $\gtrsim 1$ so that detectable X-ray line features, like the iron lines observed in several afterglows, can be produced. In this range of t_{sd} we expect a very large effective density ($\sim 10^5 \text{ cm}^{-3}$) and electron number density ($\sim 10^3 \text{ cm}^{-3}$). This effects the afterglow emission in a number of different ways: i) The self absorption frequency of the afterglow is typically above the radio, implying no detectable radio afterglow, while radio afterglows were detected for GRBs 970508, 970828, and 991216, where the iron line feature for the latest of these three is the most significant detection to date ($\sim 4\sigma$, Piro et al. 2000). We also typically expect the self absorption frequency of the plerion emission to be above the radio in this case, so that the radio emission from the plerion should not be detectable, and possibly confused with that of the afterglow. However, for a relatively large iron mass ($\sim 1 M_\odot$) we can have t_{Fe} as large as $\sim 3 - 4$ yr, which may bring the self absorption frequency of the plerion below the radio band, and thus make the radio emission from the plerion detectable (at the level of $\sim 0.1 - 1$ mJy, see Figure 1 of GG). This might provide an alternative explanation for the ‘enigmatic’ radio afterglow of GRB 991216 (Frail et al. 2000). ii) A short jet break time t_j and a relatively short non-relativistic transition time t_{NR} are implied, as both scale linearly with t_{sd} and are in the right range inferred from observations for $t_{\text{sd}} \sim 30$ yr (see Eqs. 92, 93 of GG). iii) The electrons are always in the fast cooling regime during the entire afterglow. For t_{sd} in this range the optical emission from the plerion is at the level of $F_\nu \sim 1 \mu\text{Jy}$, for $\gamma_w \lesssim 10^5$. The X-ray emission from the plerion may become detectable (i.e. \gtrsim a few $10^{-14} \text{ erg cm}^{-2} \text{ s}^{-1}$) only for $\gamma_w \lesssim 10^4$ (which is beyond the expected range for γ_w).

5. Finally, for $t_{\text{sd}} > t_{\text{Fe}}$, we expect no iron lines. When t_{sd} is between ~ 2 yr and ~ 20 yr the radio emission of the plerion may be detectable for $\gamma_w \lesssim 10^5$. The lack of detection of such a radio emission excludes values of t_{sd} in this range, if indeed $\gamma_w \lesssim 10^5$, as is needed to obtain reasonable values for the break frequencies of the afterglow. For $t_{\text{sd}} = t_{\text{ISM}} \sim 38$ yr, the effective density of the PWB is similar to that of the ISM (i.e. 1 cm^{-3}), and the afterglow emission is similar to that of the standard model, where $k = 0$ is similar to an ISM environment, with the exception that in our model a value of $k = 1$, that is intermediate between an ISM and a stellar wind, is also possible. Larger (smaller) values of the external density are obtained for smaller (larger) values of t_{sd} . The lack of detection of the EC component in the X-ray band (2 – 10 keV), except perhaps in one afterglow (GRB 000926, Harrison et al. 2001) constrains the ratio of the wind termination shock radius, R_s , and the outer radius of the PWB, R_b , to be $\lesssim 0.1 - 0.3$, for $t_{\text{sd}} \sim 10 - 30$ yr, which is a bit hard to obtain with a spherical model (KG).

3. X-ray Lines: Iron Vs. Light Elements

Recently, there have been claims for the detection of light element lines (Mg, Si, S, Ar, Ca) in the X-ray afterglow of a few GRBs (011211, Reeves et al. 2002; 001025A, 010220, Watson et al. 2002). For GRB 011211, there is no evidence for lines from intermediate mass elements such as Ni, Co or Fe (perhaps only a marginal detection of a blueshifted Ni line) and an optical afterglow has been observed (Holland et al. 2002), enabling the determination of a spectroscopic redshift, $z = 2.141 \pm 0.001$ (Fruchter et al. 2001; Gladders et al. 2001). For GRBs 001025A and 010220 there is no optical afterglow (and therefore no spectroscopic redshift), and there is an indication for an over-abundance of Ni or Co (or to our opinion, possibly Fe). Reeves et al. (2002) estimate the radius of the line producing material from the geometrical time delay, $R = t/[(1+z)(1-\cos\theta)] \approx 10^{15}$ cm, where θ is the angle from which the line photons are emitted (which is identified with the jet opening angle, θ_j) and t is the duration of the line emission. However, they used $\theta_j = 20^\circ$, while there is an indication for a jet break in the optical light curve at $t_j \approx 1.5 - 2.7$ days, which implies $\theta_j \approx 3.4 - 4.2^\circ$ (Holland et al. 2002). This increases the estimate of the radius R by a factor of $[20/(3.4 - 4.2)]^2 \sim 30$. They also estimate the duration of the line emission as 10^4 s (the time of the observation itself), while we believe that a more reasonable estimate is the time after the GRB at which the observation was made. The observation started 11 hr after the burst, while the lines are most prominent during the first 5000 s of observation. This would increase the estimate of R by a factor of $(11 \text{ hr})/(10^4 \text{ s}) \approx 4$. Altogether, we obtain $R \approx (1.4 - 2.1) \times 10^{17}$ cm, which is more than two orders of magnitude larger than the estimate of Reeves et al. (2002). The value of R may be lower if the ionizing radiation extends out to angles $\theta > \theta_j$. Therefore, there is no compelling evidence for a small radius of $R \approx 10^{15}$ cm and a correspondingly small $t_{\text{sd}} \sim R/(0.1c) \sim$ a few days, just from considerations of geometrical time delay. Instead, we obtain $t_{\text{sd}} \lesssim 1 - 2$ yr.

In order for the light element lines to be stronger than the iron lines (or Ni or Co lines for this matter), the ionization parameter should be $\xi = 4\pi F/n \lesssim 100$ (Lazzati, Ramirez-Ruiz & Rees 2002), where F is the ionizing flux (in the range 1–10 keV) and n is the number density of the line producing material. We expect a roughly similar ionizing luminosity for different GRBs, so that $F \propto R^{-2}$, while the density of the SNR shell scales as $n \propto 1/R^2 \Delta R$, implying $\xi \propto \Delta R$, where ΔR is the width of the SNR shell. We generally expect ΔR to increase with R , possibly linearly. Therefore, ξ is expected to increase with R and consequently with t_{sd} . For this reason we expect the light element lines to be more prominent for small values of t_{sd} , while Fe lines should dominate for larger values of t_{sd} (in this case we would not expect Ni or Co lines, as the latter would have had enough time to decay into Fe).

4. External Compton and High Energy Emission

An interesting new ingredient of the PWB model, is that the GRB and its afterglow occur inside a photon rich plerionic environment. These photons can be upscattered by the relativistic electrons behind the afterglow shock, producing a high energy emission (external Compton, EC). As has been shown in GG (see Figure 2 therein), for $t_{\text{sd}} = t_{\text{ISM}}$ and $R_s/R_b \lesssim 0.3$, the EC is dominant above $\sim 500 (t/1 \text{ hr})^{-1.2}$ keV (where t is the observed time after the GRB), while synchrotron is dominant at lower energies. This time dependence is valid up to $t \sim 1$ hr, while for later times the decrease with time is more moderate.

Figure 1 shows the afterglow spectrum at $t = 1$ day, for $t_{\text{sd}} = t_{\text{Fe}}$ and t_{ISM} , where for clarity, the synchrotron, synchrotron self-Compton (SSC) and EC components are shown separately. It can be seen that the EC component becomes more important for larger t_{sd} . We expect an upper cutoff due to opacity to pair production with the photons of the plerion at $h\nu_{\gamma\gamma} \sim 100(t_{\text{sd}}/t_{\text{ISM}})^2$ GeV. This latter upper cutoff moves down to a lower energy for smaller values of t_{sd} , and is ~ 100 MeV for $t_{\text{sd}} = 1$ yr $\sim t_{\text{Fe}}$, as can be seen in Figure 1. For afterglows with X-ray line features we expect no high energy emission above this limit.

For $t_{\text{sd}} \sim t_{\text{ISM}}$, the EC component dominates the early afterglow ($t \lesssim 100$ s) emission above ~ 100 MeV. At early times, the afterglow radius is relatively small and we expect the ratio, X , of energies in the EC and synchrotron components to be roughly constant in time, so that the peak of the νF_{ν} EC spectrum has a temporal scaling similar to that of the synchrotron component (i.e. $\propto t^{-1}$, see GG). We expect νF_{ν} to decay very slowly with time, as $t^{-1/4}$, for $\nu < \nu_m^{EC}$, and decay approximately linearly with time ($\propto t^{-1-3(s-2)/4}$) for $\nu > \nu_m^{EC}$. The temporal decay becomes steeper than these scalings as the afterglow radius increases and X begins to decrease with time. The EC emission can account for the high energy emission detected by EGRET for GRB 940217 (Hurley et al. 1994), and is consistent with the flux level and relatively moderate time decay observed in this case.

A different interpretation for the high energy emission discussed above was recently suggested by Wang, Dai & Lu (2002), in a similar context of the supranova model, where the GRB occurs inside a plerionic environment. However, their results imply that the typical synchrotron frequency is $h\nu_m \sim$ a few keV after one day, which is inconsistent with afterglow observations (unless GRBs with delayed high energy emission constitute a different class of GRBs, with a very different afterglow emission).

5. An Elongated Geometry

For a spherical PWB, the X-ray features observed in several afterglows cannot be reconciled with the conventional afterglow emission observed in the same afterglows. However, this discrepancy may be reconciled if the PWB is elongated along its rotational axis, so that the polar radius is much larger than the equatorial radius. One may naturally expect such a geometry for a number of different reasons (KG; GG). In this case the iron lines can be emitted by clumpy SNR material at small radii, near the equator, while the afterglow emission originates from along the polar direction, where the GRB outflow is expected to propagate, and may reach a considerably larger radius. In this picture, the effective density within the PWB is relatively small, close to that of a sphere with the polar radius. This helps reproduce the typical afterglow emission, and avoid direct detection of the plerion emission in the radio. Another advantage of an elongated geometry is the suppression of the EC component in the X-ray afterglow, that results since a ratio of $R_s/R_b \lesssim 0.1$ is naturally expected in this case.

6. Conclusions

In this work we have presented the main observational implications for GRBs that occur inside pulsar wind bubbles (PWBs), as expected in the supranova model. We have examined the relations between the different observations and put the different ingredients of the model into one coherent framework.

We find that a simple spherical model cannot produce the iron line features observed in several afterglows together with the other, more conventional, features of the afterglow emission from these bursts. However, if the iron lines are not real, then a simple spherical model can explain all other observations for $t_{\text{sd}} \gtrsim 20$ yr. The latter is required in order to explain typical afterglow observations and the lack of direct detection of the plerion emission in the radio during the afterglow.

If the iron line detections are real, then in the context of the PWB model, this requires deviations from a simple spherical geometry. The most straightforward variation of the simple model is a PWB that is elongated along its polar axis. Such a geometry may arise naturally within the context of this model (KG; GG).

With an elongated geometry, the PWB model can account for all the observed features in the afterglow, and it offers a number of advantages in comparison to other models: i) It provides a relatively baryon clean environment for the GRB jet, which is required in order to produce a highly relativistic outflow. This arises as the initial supernova expels most of

the stellar envelope to a large distance from the site of the GRB, and the strong pulsar wind effectively sweeps up the remaining baryonic matter. ii) An important advantage of this model is that it can naturally explain the large values of ϵ_B and ϵ_e that are inferred from fits to afterglow data (KG), thanks to the large magnetic fields in the PWB and the large relative number of electron-positron pairs. This is in contrast with standard environment that is usually assumed to be either an ISM or the stellar wind of a massive progenitor, that consists of protons and electrons in equal numbers. In this case, the pre-existing magnetic field, that is amplified due to the compression of the fluid in the shock, is too small to explain the values inferred from afterglow observations, and further magnetic field amplification or generation at the shock is required. iii) All the detections of GRB afterglows to date are for the long duration sub-class of GRBs (with a duration $\gtrsim 2$ s), that are believed to arise from a massive star progenitor, which according to the collapsar model should imply a stellar wind environment ($k = 2$). However, a homogeneous external medium ($k = 0$) provides a better fit to the observational data for most GRB afterglows. This apparent contradiction is naturally explained in the context of the PWB model, where k ranges between 0 and 1, while we still have a massive star progenitor. iv) Another advantage of the PWB model is its capability of explaining the high energy emission observed in some GRBs (Schneid et al. 1992; Sommer et al. 1994; Hurley et al. 19994; Schneid et al. 1995). We find that the high energy emission during the early afterglow at photon energies $\gtrsim 100$ keV is dominated by the EC component. We predict that such a high energy emission may be detected in a large fraction of GRBs with the upcoming mission GLAST. However, we find an upper cutoff at a photon energy of $\sim 100 (t_{\text{sd}}/1 \text{ yr})^2$ MeV, due to opacity to pair production with the photons of the PWB. This implies no high energy emission above ~ 100 MeV for afterglows with X-ray line features, but allows photons up to an energy of ~ 100 GeV for afterglows with an external density typical of the ISM ($t_{\text{sd}} \sim 38$ yr).

We thank Arieh Königl for many helpful discussions. This research was supported by the Institute for Advanced Study, funds for natural sciences (JG). We thank the Einstein Center at the Weizmann Institute of Science for the hospitality and for the pleasant working atmosphere. DG thanks the Institute for Advanced Study, where most of this research was carried out, for the hospitality and the nice working atmosphere.

REFERENCES

Eichler, D., et al. 1989, *Nature*, 340, 126

Frail, D., et al. 2000, *ApJ*, 538, L129

Fruchter, A., et al. 2001, GCN Circ. 1200

Fryer, C., & Woosley, S.E. 1998, ApJ, 502, L9

Fryer, C., Woosley, S.E., & Hartmann, D.H. 1999, ApJ, 526, 152

Gladders, M., et al. 2001, GCN, Circ. 1209

Guetta, D., & Granot, J. 2002, submitted to MNRAS (astro-ph/0208156), (GG)

Harrison, F.A., et al. 2001, ApJ, 559, 123

Holland, S.T., et al. 2002, AJ, 124, 639

Hurley, K., et al. 1994, Nature, 372, 652

Inoue, S., Guetta, D., & Pacini, F. 2002, ApJ in press (astro-ph/0111591)

Königl, A., & Granot, J. 2002, ApJ, 574, 134

Lazzati, D., Campana, S., & Ghisellini, G. 1999, MNRAS, 304, L31

Lazzati, D., Ramirez-Ruiz, E., & Rees, M.J. 2002, ApJ, 572, L57

Narayan, R., Paczński, B., & Piran, T. 1992, ApJ, 395, L83

Paczński, B. 1998, ApJ, 494, 45

Piro, L., et al. 2000, Science, 290, 955

Reeves, J.N., et al. 2002, Nature, 416, 512

Schneid, E.J., et al. 1992, A&A, 255, L13

Schneid, E.J., et al. 1995, ApJ, 453, 95

Sommer, M., et al. 1994, ApJ, 422, L63

Vietri, M. & Stella, L. 1998, ApJ, 507, L45

Vietri, M., et al. 2001, ApJ., 550, L43

Wang, X.Y., Dai, Z.G., & Lu, T. 2002, accepted to MNRAS (astro-ph/0206499)

Watson, D., et al. 2002, A&A, 393, L1

Woosley, S.E. 1993, ApJ, 405, 273

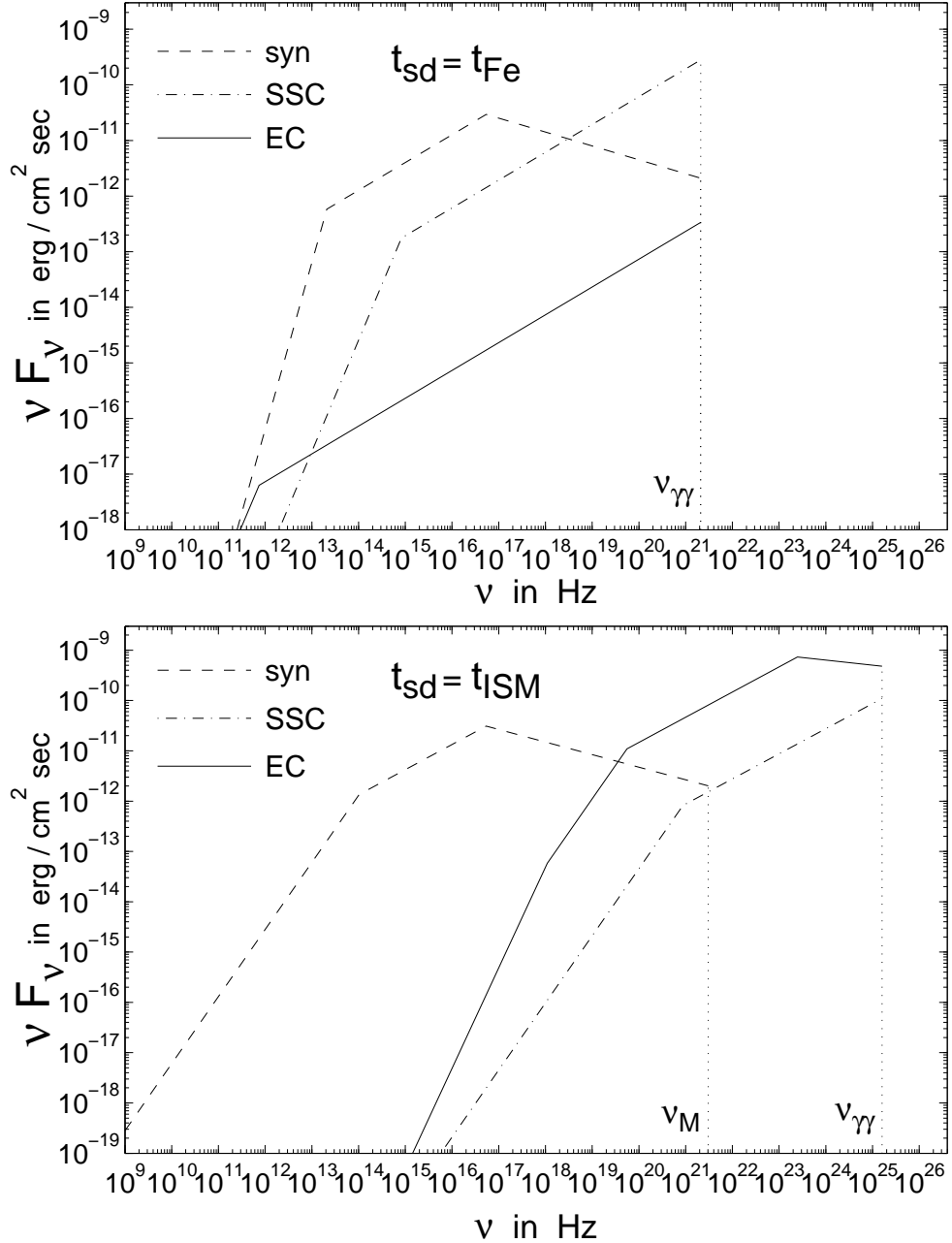


Fig. 1.— The afterglow spectrum at one $t = 1$ day after the GRB, for $t_{\text{sd}} = t_{\text{Fe}} \sim 1$ yr (upper panel) and for $t_{\text{sd}} = t_{\text{ISM}} \sim 38$ yr (lower panel), calculated for the fiducial parameters of Guetta & Granot (2002). Dotted vertical lines indicate ν_M where the upper cutoff for the synchrotron emission is located (e.g. GG), and $\nu_{\gamma\gamma}$ where the upper cutoff of the SSC and EC (due to pair opacity) is located.